Asteroid 21 Lutetia: Low Mass, High Density

Asteroid (21) Lutetia – low mass, high density

M. Pätzold (1), T. P. Andert (2), S.W. Asmar (3), J.D. Anderson (3), J.-P. Barriot (4), M.K. Bird (5), B. Häusler (2), M. Hahn (1), S. Tellmann (1), H. Sierks (6), P. Lamy (7), B.P. Weiss (8)

(1) Rheinisches Institut für Umweltforschung, Abt. Planetenforschung, an der Universität zu Köln, Cologne, Germany

(2) Institut für Raumfahrttechnik, Universität der Bundeswehr München, Neubiberg, Germany

(3) Jet Propulsion Laboratory, Caltech, Pasadena, California, USA

(4) Géosciences du Pacifique Sud, Université de la Polynésie Française, BP 6570, 98702 FAA'A, Tahiti, Polynésie Francaise

(5) Argelander Institut für Astronomie, Universität Bonn, Bonn, Germany

(6) Max-Planck-Institut für Sonnensystemforschung, Katlenburg-Lindau, Germany

(7) Laboratoire d'Astrophysique de Marseille, Marseille, France

(8) Dept. of Earth, Atmospheric and Planetary Sciences, Massachusetts Institute of Technology, Cambridge, MA, USA

The additional Doppler shift of the Rosetta spacecraft radio signals imposed by Lutetia's gravitational perturbation on the flyby trajectory are used to determine the mass of the asteroid. Calibrating and correcting for all Doppler contributions not associated with Lutetia, a least-squares fit to the residual frequency observations from four hours before to six hours after closest approach yields a mass of (1.700 +/- 0.017)·10^{18} kg (error: 1.0%). Using the volume model of Lutetia determined by the Rosetta OSIRIS camera, the bulk density, an important parameter for clues to its composition and interior, is (3.4 +/- 0.3)·10^3 kg/m^3.

Asteroid (21) Lutetia, discovered in 1852, is one of the larger main belt asteroids. In 2004, it became the flyby target asteroid for the Rosetta mission. An important characteristic of an asteroid is its bulk density, derived from its mass and its volume. Although there are a number of asteroid mass determination techniques, by far the most accurate is spacecraft tracking during a close flyby.

The velocity of a spacecraft flying by a body of sufficient size and at a sufficiently close distance is perturbed by the attracting force of that body. The perturbed velocity is estimated from the additional Doppler shift of the transmitted radio signal in comparison with the expected Doppler shift of an unperturbed trajectory (1).

The Rosetta flyby geometry at Lutetia on 10 July 2010 was suboptimal because of the large flyby distance d=3168 +/- 7.5 km, the high relative flyby velocity v_0=14.99 km/s and the projection angle between the relative velocity and the direction to Earth of α=171.2°, all of which reduced the post-encounter amplitude of the expected Doppler shift.

The final Doppler frequency shift six hours after the closest approach after correcting for contributions not associated with Lutetia (see Supporting Online Material SOM) is Δf=36.2±0.2 mHz (Figure 1). The value of *GM* from a least-squares fitting procedure and considering further error sources is determined to be $GM=(11.34\pm0.11)\cdot10^{-2}$ km^3s^{-2}, corresponding to a mass of $(1.700\pm0.017)\cdot10^{18}$ kg (error: 1.0%). The uncertainty in *GM* considers the error from the least squares fit mainly driven by the frequency noise (0.55%), the uncertainty in the Lutetia ephemeris introduced by the uncertainty in the flyby distance of ±7.5 km (0.24%) and the considered uncertainty in the tropospheric correction introduced by the zenith delay model and the mapping function of the ground station elevation (0.8%). These contributions yield a total uncertainty of 1.0%. The values for *GM* and Δf agree within the error with the analytical solution (2). The derived mass is lower than other mass determinations of Lutetia from astrometry (see SOM).

One of the most important global geophysical parameters, which provide clues to the origin, internal structure and composition of Lutetia, is the mean (bulk) density, derived from the mass and the volume. Observations of the OSIRIS camera and ground observations using adaptive optics were combined to model the global shape.. The derived volume is $(5.0\pm0.4)\cdot10^{14}$ m^3 (4). The volume leads to a bulk density of $(3.4 \pm 0.3)\cdot10^3$ kg/m^3. This high bulk density is unexpected in view of the low value of the measured mass. It is one of the highest bulk densities known for asteroids (5). Assuming that Lutetia has a modest macroporosity of 12%, it would imply that the bulk density of its material constituents would exceed that of stony meteorites. Unless Lutetia has anomalously low porosity compared to other asteroids in its size range, its high density likely indicates a nonchondritic bulk composition enriched in high atomic number like iron. It may also be evidence for a partial differentiation of the asteroid body as proposed by Weiss et al. (6).

Notes:

(1) Andert, T.P., P. Rosenblatt, M. Pätzold, B. Häusler, V. Dehant, G. L. Tyler, and J. C. Marty, Precise mass determination and the nature of Phobos, Geophysical Research Letters, Volume 37, Issue 9, CiteID L09202, 2010.

(2) As shown in (3), the expected final post-encounter Doppler shift of a two-way radio carrier signal is (α'=172.18° is the direction to Earth projected into the flyby plane, β=3° is the direction angle to Earth above the flyby plane)

$$\Delta f\left(t \rightarrow \infty\right) = 4\frac{f_X}{c}\frac{GM}{d \cdot v_0} \cdot \sin\alpha' \cos\beta$$

Using the fit solution for Lutetia of GM = (11.34±0.11)·10^{-2} km^3/s^2 the analytical result of the relation above is (36.4±0.4) mHz.

(3) Pätzold, M., T. P. Andert, B. Häusler, S. Tellmann, J. D. Anderson, S. W. Asmar, J.-P. Barriot, and M. K. Bird, Pre-flyby estimates of the precision of the mass determination of asteroid (21) Lutetia from Rosetta radio tracking, Astronomy and Astrophysics, Volume 518, id.L156, 2010. (4) Sierks et al., this issue, 2011.

(5) Similar high bulk densities are known for the asteroids (4) Vesta, (16) Psyche, (20) Massalia, (22) Kalliope, all larger than Lutetia. Bulk densities of more primitive C-type asteroids are in the range 1200 kg/m^3 to 2700 kg/m^3.

(6) Weiss, B.P., L.T. Elkins-Tanton, M.A. Barucci, H. Sierks, M. Pätzold, C. Snodgrass, S. Marchi, I. Richter, P.R. Weissman, M. Fulchignoni and R.P. Binzel, Evidence for thermal metamorphism or partial differentiation of asteroid 21 Lutetia from Rosetta, 42nd Lunar and Planetary Science Conference, 2077, (2011)..

The Rosetta Radio Science Investigation (RSI) experiment is funded by DLR Bonn under grants 50QM1002 (TA, BH) and 50QM1004 (MP, MH, ST, MKB) and under a contract with NASA (SWA, JDA). We thank T. Morley for valuable comments and all persons involved in Rosetta at ESTEC, ESOC, ESAC, JPL and the ESTRACK and DSN ground stations for their continuous support.

Figure Captions:

Figure 1: Filtered and adjusted frequency residuals at X-band from 4 hours before closest approach to 6 hours after closest approach. Two tracking gaps (light red shaded zones) are indicated from 5 minutes before closest approach to 45 minutes after closest approach as planned and from 192 minutes to 218 minutes after closest approach when DSS 63 accidentally dropped the uplink. The red solid line is a least-squares fit to the data from which *GM* is determined.

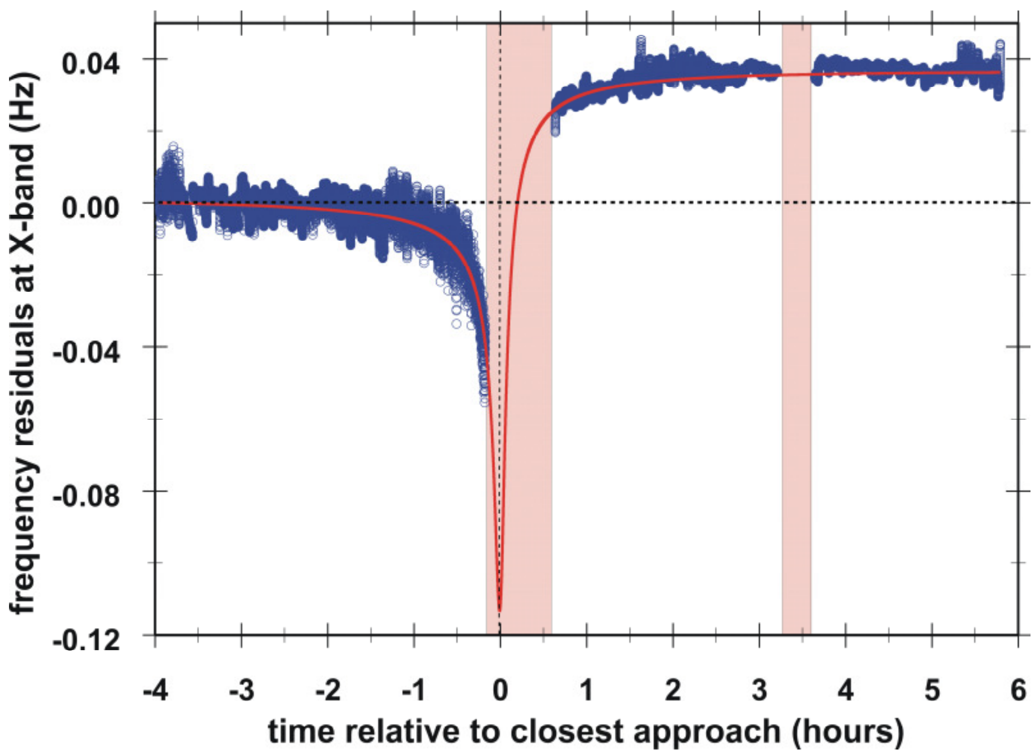

Asteroid (21) Lutetia – low mass, high density

Supporting Online Material

M. Pätzold (1), T. P. Andert (2), S.W. Asmar (3), J.D. Anderson (3), J.-P. Barriot (4), M.K. Bird (5), B. Häusler (2), M. Hahn (1), S. Tellmann (1), H. Sierks (6), P. Lamy (7), B.P. Weiss (8)

(1) Rheinisches Institut für Umweltforschung, Abt. Planetenforschung, an der Universität zu Köln, Cologne, Germany

(2) Institut für Raumfahrttechnik, Universität der Bundeswehr München, Neubiberg, Germany

(3) Jet Propulsion Laboratory, Caltech, Pasadena, California, USA

(4) Géosciences du Pacifique Sud, Université de la Polynésie française, BP 6570, 98702 FAA'A, Tahiti, Polynésie Francaise

(5) Argelander Institut für Astronomie, Universität Bonn, Bonn, Germany

(6) Max-Planck-Institut für Sonnensystemforschung, Katlenburg-Lindau, Germany

(7) Laboratoire d'Astrophysique de Marseille, Marseille, France

(8) Dept. of Earth, Atmospheric and Planetary Sciences, Massachusetts Institute of Technology, Cambridge, MA, USA

The additional Doppler shift of the Rosetta spacecraft radio signals imposed by Lutetia's gravitational perturbation on the flyby trajectory are used to determine the mass of the asteroid. Calibrating and correcting for all Doppler contributions not associated with Lutetia, a least-squares fit to the residual frequency observations from four hours before to six hours after closest approach yields a mass of (1.700 +/- 0.017)·10^{18} kg (error: 1.0%). Using the volume model of Lutetia determined by the Rosetta OSIRIS camera, the bulk density, an important parameter for clues to its composition and interior, is (3.4 +/- 0.3)·10^{3} kg/m^{3}.

1. Flyby and Observation

The Rosetta spacecraft was tracked during the flyby at asteroid 21 Lutetia on 10 July 2010 with NASA´s Deep Space Network (DSN) 70-m antenna (DSS 63) near Madrid, Spain. Strong carrier signals at X-band (f_X=8.4 GHz) and S-band (f_S=2.3 GHz) were received throughout the flyby (Figure 1) except for a planned tracking gap from 5 minutes before closest approach (t_0) to 40 minutes after t_0 and a short gap of 26 minutes starting at 192 minutes after t_0, when the uplink was accidentally dropped at DSS 63. The sampling time during the 10 hours of recording was one sample per second.

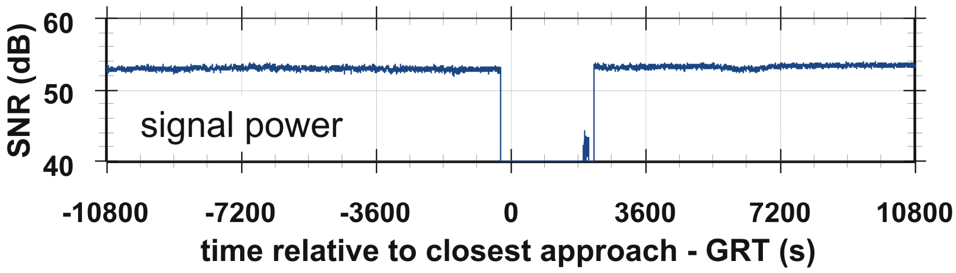

Figure 1: Received signal power at X-band from Rosetta +/- 3 hours around closest approach.

2. Frequency Prediction

The received carrier frequency from the actual flyby is compared with a carrier frequency prediction of a spacecraft motion unperturbed by the asteroid. This frequency prediction is based on a complex force model taking into account gravitational forces (Folkner et al., 2008) from the Sun and planets, and the largest asteroids Ceres, Pallas and Vesta, but <u>not</u> the target asteroid, and non-gravitational forces acting on the spacecraft (e.g. solar radiation pressure relative to a spacecraft macro-model with known optical parameters of each plane and the solar panels and their orientation at each time step). Also required are precise knowledge of the location of the ground station antenna phase center, and its behavior under forces like solid Earth tides and plate tectonic and a function of Earth rotation, precession and nutation (McCarthy & Petit, 2003),. Relativistic propagation effects are considered up to second order (Häusler et al., 2007).

The frequency prediction is routinely computed for radio science data processing on the Mars Express and Venus Express missions (Pätzold et al., 2002).

3. Frequency residuals

The frequency shift from the perturbed spacecraft motion caused by the attracting force of the asteroid is extracted from the frequency recorded in the ground station on Earth by subtracting the predicted unperturbed frequency. The difference between the observed perturbed and the predicted unperturbed Doppler shift is the raw frequency residual (Figure 2a).

Figure 2 (next page): Frequency residuals at X-band from t_0-4 hours to t_0+6 hours. Two tracking gaps are indicated (light red shaded zones) from t_0-5 minutes to t_0+45 minutes as planned and from t_0+192 minutes to t_0+218 minutes when DSS 63 accidentally dropped the uplink. a) raw uncalibrated frequency residuals (observed frequency minus predicted frequency). These raw residuals must be corrected for tropospheric propagation (solid line). b) Frequency residuals after tropospheric correction. The feature between t_0+95 minutes and t_0+165 minutes was caused by an HGA slew in elevation and azimuth, thereby producing an additional velocity component along the line-of-sight. c) HGA slew rates in azimuth (red) and elevation (blue). It is evident that the HGA generated an additional Doppler shift at the highest slew rates, in particular starting at t_0-15 minutes. These contributions overcompensated the Doppler shift from the gravitational attraction of the asteroid. d) Frequency residuals corrected for the HGA slew rates. The large positive frequency residuals just before the first tracking gap are caused by the abrupt stop of the HGA slew. e) Filtered frequency residuals to reduce noise. The red solid line is a least-square fit to the data from which *GM* is determined.

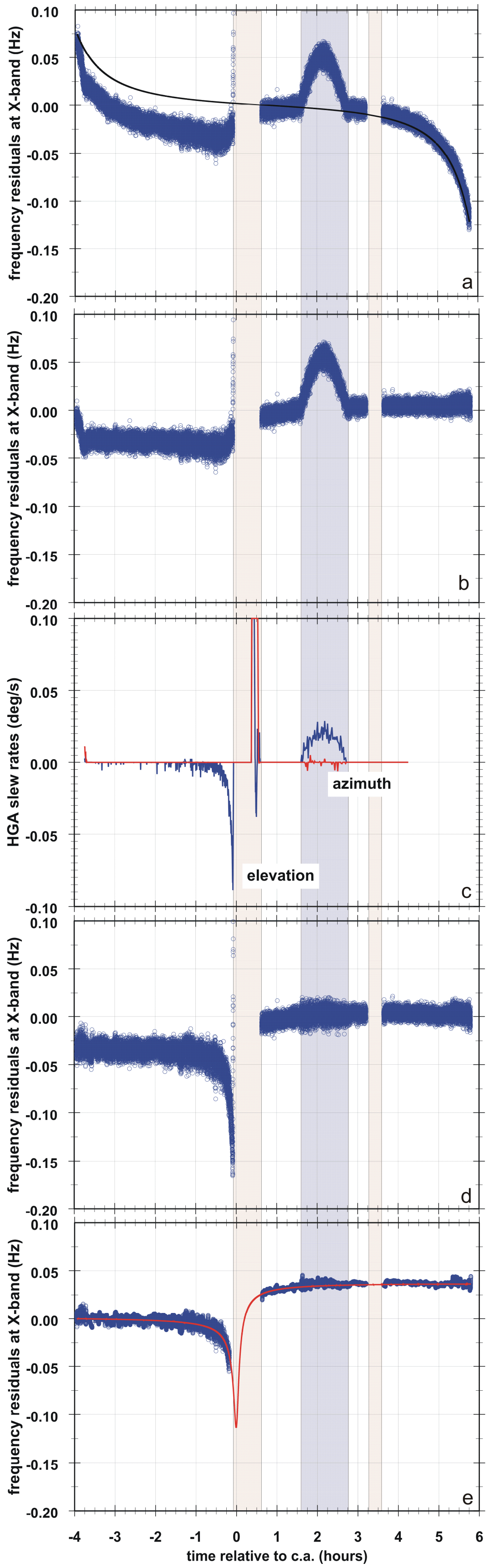
0.10
0.05
0.00
-0.05
-0.10
-0.15
-0.20
frequency residuals at X-band (Hz)
a
b
HGA slew rates (deg/s)
azimuth
elevation
c
d
e
-4
-3
-2
-1
0
1
2
3
4
5
6
time relative to c.a. (hours)

Figure 2

4. Tropospheric correction

The raw frequency residuals during the flyby contain a contribution caused by the propagation of the radio signal through the Earth's troposphere. The propagation is mainly affected by the temperature, the atmospheric pressure and the partial pressure of water vapor. These meteorological parameters are recorded at the ground station site and used for calibration.

The tropospheric refraction of the radio ray path in the Earth atmosphere consists of two components: i) the dry component, the non-water-vapor component of the atmosphere, and ii) the contribution of the highly variable water vapor content of the atmosphere(the so-called wet component). The correction for refraction in the Earth's atmosphere is calculated with models for the path delay and mapping functions which project the path delay onto the direction of the signal path for the wet and dry components.

The models from Saastamoinen et al. (1972) for the dry component, from Ifadis (1986) for the wet component, and the straightforward mapping functions from (Chao, 1972) were used to compute the tropospheric correction. The uncertainty in the wet component is much larger than that of the dry component.

The tropospheric correction is subtracted from the raw frequency residual (Figure 2a) to obtain the tropospherically corrected residual (Figure 2b). The difference between three correction models (Schüler, 2001, Boehm et al., 2006, Petit and Luzum, 2010) for the zenith delay and mapping functions was used to derive an systematic error estimate of the GM derivation.

5. High Gain Antenna motion

The steerable High Gain Antenna (HGA) of the spacecraft maintained Earth pointing until five minutes before closest approach, at which time the end position of the HGA motion was reached. The readjustment of the HGA resulted in a tracking gap of 45 minutes, including the time of closest approach. Pre-encounter flyby simulations, however, showed that stable and precise solutions for the mass can be achieved even with tracking gaps of several hours (Pätzold et al., 2010). While the Rosetta on-board instruments continued to track the asteroid, the HGA was articulated to reacquire Earth pointing. The varying HGA slew rates in azimuth and elevation (Figure 2c) induced an extra Doppler shift along the line-of-sight (LOS), which began to become significant at 15 minutes before closest approach.

The rotation of the steerable HGA during the flyby induced an additional frequency shift on the observed radio signal which needs to be removed. This is done by applying the LOS component of $\Delta \boldsymbol{v} = \boldsymbol{\omega} \times \boldsymbol{r}$, where $\boldsymbol{r}$ is the vector from the center of mass (COM) to the phase center of the antenna and $\boldsymbol{\omega}$ the rotation rate of the antenna. Because the COM changed during the motion of the HGA, the location of the COM was adjusted during the fitting process.

To demonstrate this motion correction, we used a pre-planned HGA motion maneuver performed in 2004. The HGA was rotated from -95° to -23° in elevation with a maximum elevation rotation rate of 0.1°/sec and from -34° to 34° in azimuth with a maximum azimuth rotation rate of 0.03°/sec (Figure 3). The maximum resulting frequency shift caused by the antenna rotation is about 300 mHz (Figure 4). The frequency shift caused by the antenna motion was corrected by using the above model and the resulting residuals are shown in Figure 5. It is seen that the frequency noise increased during the rotational motion caused by short term variations in the rotation rate. The additional frequency shift induced by the rotation of the HGA, however, is essentially removed from the frequency residuals, which are distributed about a mean value of zero.

The Doppler contributions from the HGA slew are evident in Figure 2b. The increase in frequency shortly before closest approach contrasts with the expected (Pätzold et al., 2010) Doppler shift signature of the asteroid. The post-encounter feature between 95 min and 165 min is a specially designed spacecraft slew for Philae observations. The contributions from the HGA slewing motion are removed to obtain the frequency residuals in Figure 2d, the calibrated and corrected Doppler shift caused by the asteroid between four hours before and six hours after closest approach.

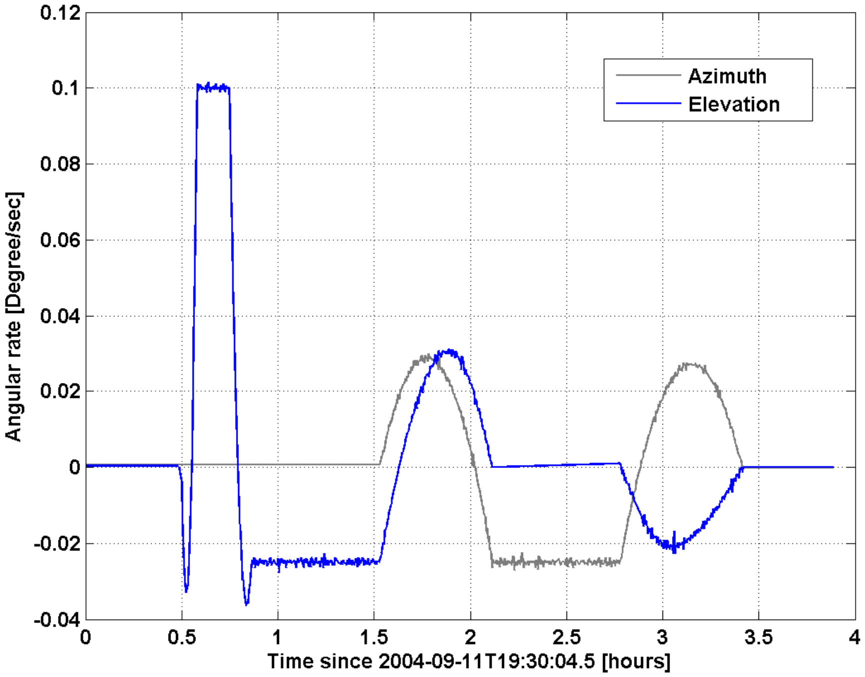

Figure 3: Angular rates of the antenna motors in elevation and azimuth during a pre-planned maneuver in 2004. These values have been provided via the spacecraft housekeeping telemetry data.

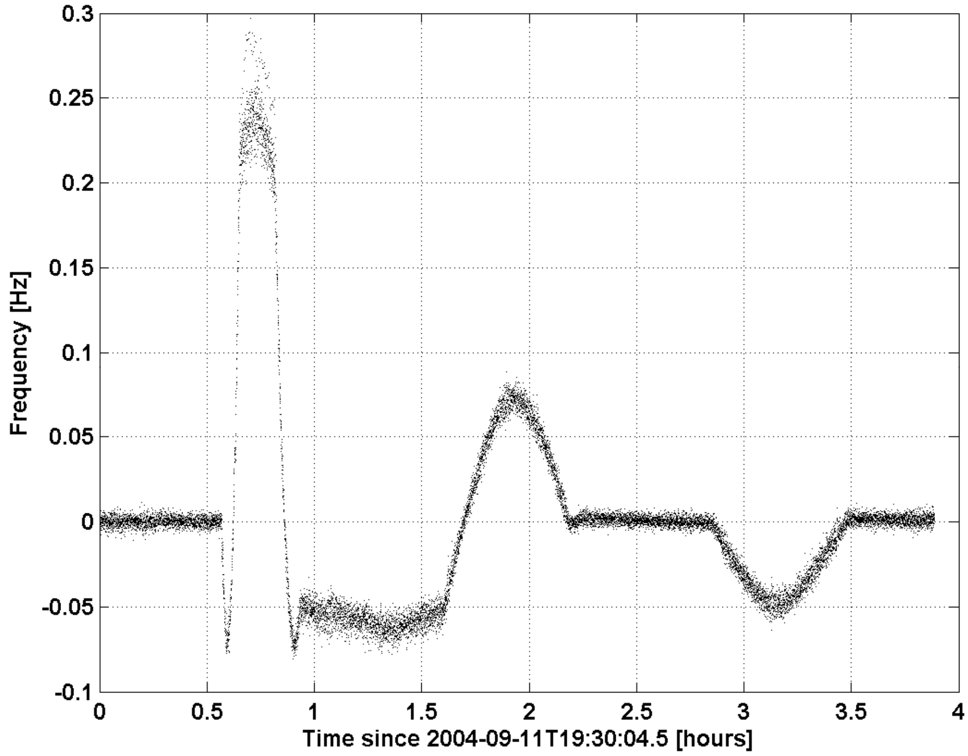

Figure 4: Residual Doppler shift at X-band after subtracting the predicted frequency during the pre-planned maneuver in 2004. The large additional Doppel frequency shift is caused by the HGA motion in azimuth and elevation..

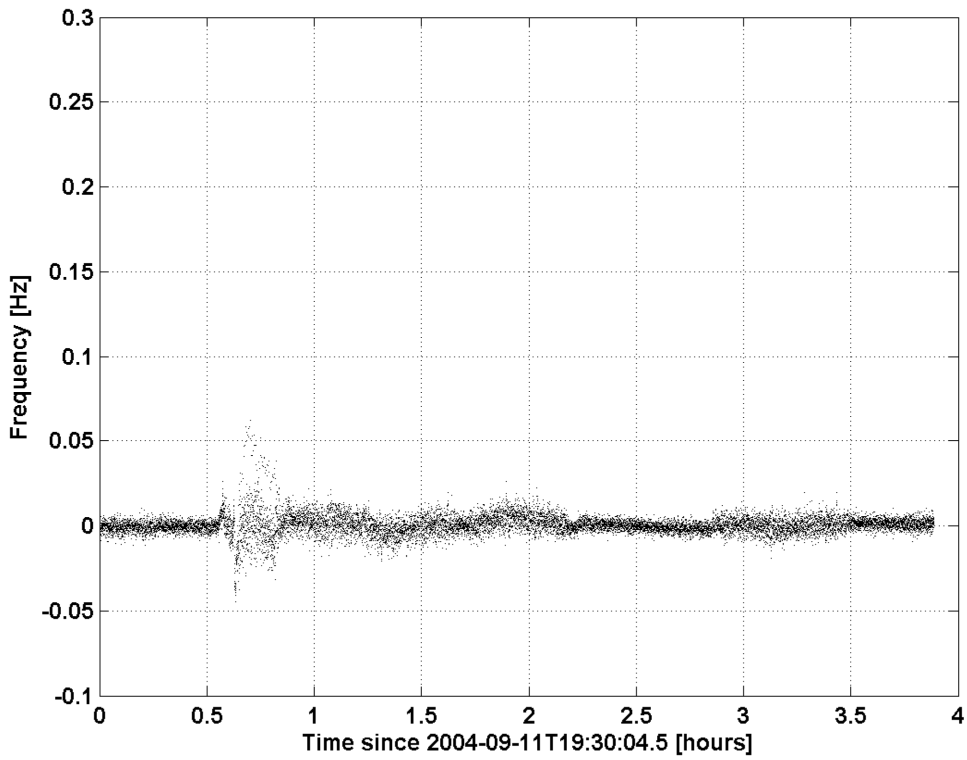

Figure 5: Residual Doppler shift from the pre-planned maneuver in 2004 after correcting with the rotation rates of the HGA antenna motors in azimuth and elevation. The rotation rates and angles were provided via the spacecraft housekeeping telemetry data.

6. Filtering and adjustment

The frequency residuals in Figure 2d were filtered at an integration time of 18 seconds for noise reduction.

Two different types of filters are used for data noise reduction: a Kaiser window filter and a moving average filter (Buttkus, 2000). Both filters are applied consecutively in forward and reverse direction ensuring a zero phase. The cut-off frequency f_c = 0.028 Hz Kaiser window filters and the integration time Δt = 18 seconds of the moving average filter were determined a priori with respect to the mass sensitivity. This approach avoids elimination of information in the data about the mass of the body and ensures that only noise is removed. The noise of the Lutetia flyby data was reduced in this step by more than a factor of two from 5.7 mHz to 2.6 mHz.

It is known from our experience with Mars Express and Venus Express radio science data processing that the frequency residuals can show a constant pre-event bias on the order of 10…50 mHz caused by contributions not considered in the prediction. In the Lutetia case, these contributions are not connected with the attracting force of the asteroid. The pre-encounter frequency residual bias of -32 mHz has been removed. This adjustment assumes a zero mean for the pre-encounter frequency residuals from t_0-4 hours to t_0-3 hours. The Hill sphere of influence of Lutetia (radius: 25,000 km) was entered at t_0-0.5h.

7. Fit and uncertainty

A least squares fit to the filtered curve (Figure 2e) yields a solution for *GM*, an adjusted pre-encounter state vector, an adjusted solar radiation pressure constant and the scale factor for the motion of the HGA phase center with respect to the spacecraft center-of-mass.

The final Doppler frequency shift six hours after the closest approach is Δf = (36.2 +/- 0.2) mHz (Figure 2e).

The mass and the other parameters were estimated with a weighted least-squares method. The initial velocity vector, the scale factor for the solar radiation pressure, the center of mass adjustment factor and the mass of Lutetia were fit using the frequency residuals. An initial state vector of the Rosetta spacecraft at t_0-4 hours is taken from the most actual SPICE-kernel[1] provided by the ESOC Flight Dynamics team as a first guess for the fitting procedure.

The change δx of the initial parameter set x iteratively aligning the measurement and the model is obtained from

$$\delta \boldsymbol{x} = (\boldsymbol{J}^T\boldsymbol{W}\boldsymbol{J} + \boldsymbol{I}\alpha)^{-1}\, \boldsymbol{J}^T\boldsymbol{W}\boldsymbol{\varepsilon}\,,$$

where $\boldsymbol{J}$ is the Jacobi matrix, containing the partial derivatives of parameter set x, $\boldsymbol{W}$ the weighting matrix containing the standard deviation of the measurement, $\boldsymbol{\varepsilon}$ the difference between model and measurement, $\boldsymbol{I}$ the identity matrix and α is a damping factor. The damping factor serves as a numerical stabilization of the solution against ill-posed parameters (Aster et al., 2005). The iterative process is applied until the solution converges, i.e. measurement and models are aligned. The inverse of the term in parenthesis is computed using singular value decomposition (Press et al., 1986).

The error of each parameter is derived from the diagonal terms of the covariance matrix

$$\boldsymbol{P} = (\boldsymbol{J}^T\boldsymbol{W}\boldsymbol{J})^{-1}.$$

The value of GM from the above described fitting procedure and considering further error sources is determined to be GM = (11.34 ±

[1] The SPICE Kernel ORHR_______________00109.BSP is available from ssols01.esac.esa.int for all Rosetta experiment teams and is considered as a long term planning orbit file for experimental purposes.

0.15)·10^{-2} km^3s^{-2} corresponding to a mass of (1.700 ± 0.017)·10^{18} kg (error: 1.3%). The uncertainty in *GM* considers the error from the least squares fit mainly driven by the frequency noise (0.55%), the uncertainty in the Lutetia closest approach time introduced by the uncertainty in the flyby distance of +/-7.5 km (0.24%) and the considered uncertainty in the tropospheric correction introduced by the mapping function of the ground station elevation (0.8%) yielding a total uncertainty of 1.0%.

The post-fit Doppler residuals, the difference observation minus the fit are shown in Figure 6.

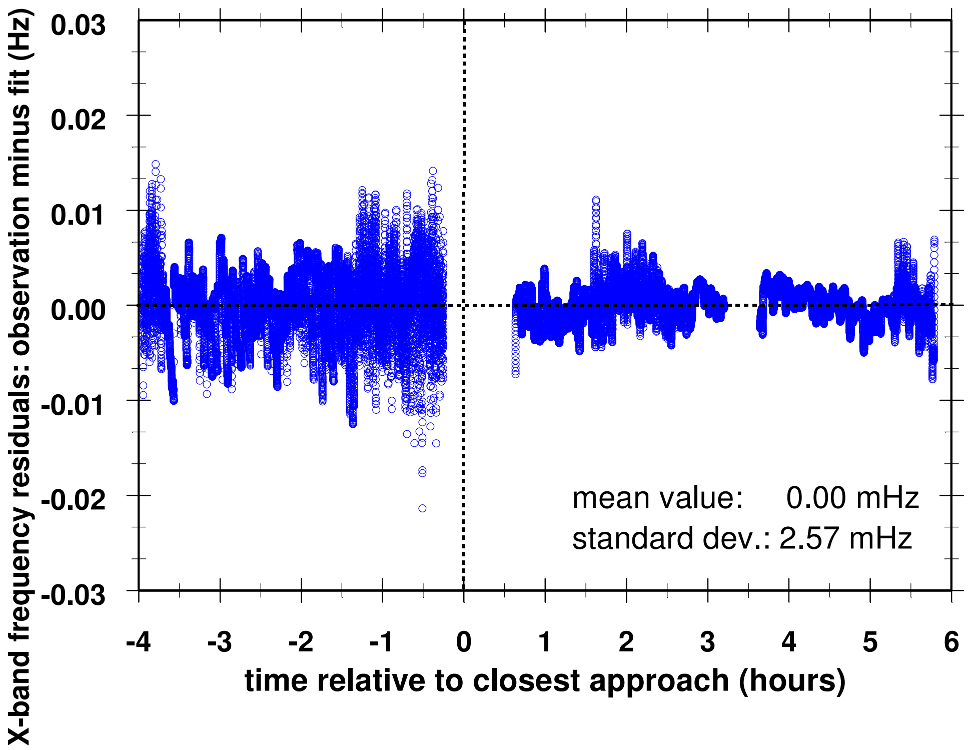

Figure 6: Post-fit residuals after subtracting the least-squares fit from the filtered observation (Figure 2e).

8. Comparison and discussion

The values for *GM* and *Δf* agree within the error with the analytical solution. As shown in (Pätzold et al., 2010), the expected final post-encounter Doppler shift of a two-way radio carrier signal is

$$\Delta f\left(t \to \infty\right) = 4\frac{f_X}{c}\frac{GM}{d \cdot v_0} \cdot \sin\alpha' \cos\beta$$

α'=172.18° is the direction to Earth projected into the flyby plane, β=3° is the direction angle to Earth above the flyby plane.

Using the fit solution for Lutetia of *GM* = (11.34±0.11)·10^{-2} km^3/s^2 the analytical result of the relation above is (36.4±0.4) mHz.

The mass estimate from the Rosetta flyby is compared in Figure 7 with the asteroid masses derived from astrometry or perturbation calculations. The derived mass is lower than other mass determinations of Lutetia from astrometry (Baer et al., 2011; Fienga et al., 2008; Fienga et al., 2010; Folkner et al., 2009). A systematic bias is apparent: Baer et al. (2010) derived a mass value of (2.59 ± 0.24)·10^{18} kg for Lutetia from asteroid/asteroid perturbations, which is 70% larger and has an error of 15%. A more recent derivation (Baer et al., 2011) yields (2.6±0.87)·10^{18} kg where the error increased by a factor of 3. Fienga et al. (2008) derived a mass value of (2.06 ± 0.6)·10^{18} kg from the influence of Lutetia on the motion of the planet Mars, which is 20% larger than Baer et al. (2010) and has an uncertainty of 30%. Again, a more recent derivation (Fienga et al., 2010) of (2.55 ± 2.34)·10^{18} kg is closer to Baer et al. (2008, 2011) but has an error of 92%. The Jet

Propulsion Laboratory (JPL) ephemeris DE421 (Folkner et al., 2009) lists the mass of Lutetia as $(2.094 \pm 0.21)\cdot 10^{18}$ kg with an error of 10%. Each precise direct mass determination of a large asteroid is therefore a valuable contribution to solar system dynamics.

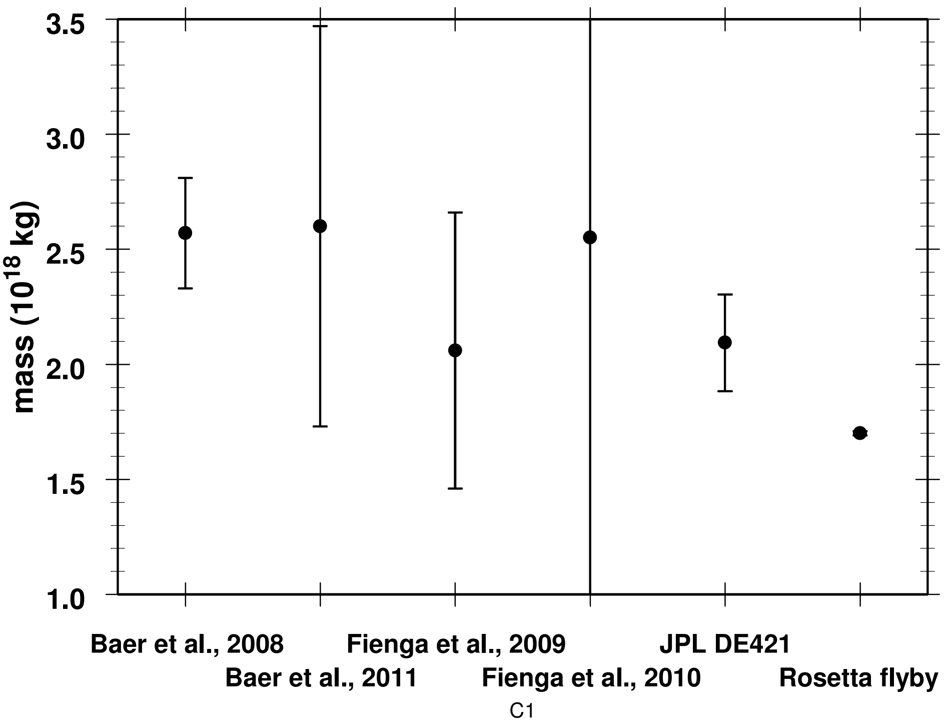

Figure 7: Comparison between mass determinations of (21) Lutetia by astrometry and the Rosetta direct mass determination. The Rosetta error bar is smaller than the measurement point. The earlier derived values are systematically higher.

The most important global geophysical parameter, which provides clues for the origin, internal structure and composition of Lutetia, is the mean (bulk) density, derived from the mass and the volume. The different pre-encounter values for the volume, as discussed earlier, vary over large ranges of the order of 20%. The precise mass value from Doppler observations during the Rosetta flyby leaves the volume as the only significant error source for the bulk density. Observations of the

OSIRIS camera and ground observations using adaptive optics were combined to model the global shape. The derived volume is (5.0 ± 0.4) 10^{14} m^3 (Sierks et al., 2011). A large part of the asteroid could not be observed during the flyby itself but the combination with adaptive optics images from other viewing directions than from the flyby, the requirement of principal axis rotation and the agreement with the KOALA (Carry et al., 2010) model with the imaged part of the asteroid constrain the error in the volume to 8%. Although the absolute value of the volume determined by Lamy et al. (2010) is confirmed, the error decreased by little more than a factor of 2.

The volume leads to a bulk density of (3.4 ± 0.3)·10^3 kg/m^3. The high bulk density is unexpected in view of the low value of the measured mass. It is one of the highest bulk densities known for asteroids. Assuming that Lutetia has a modest macroporosity of 12%, it would imply that the bulk density of its material constituents would exceed that of stony meteorites. Unless Lutetia has anomalously low porosity compared to other asteroids in its size range, its high density likely indicates a nonchondritic bulk composition enriched in high atomic number like iron. It may also be evidence for a partial differentiation of the asteroid body as proposed by Weiss et al. (2011)

Acknowledgements

The Rosetta Radio Science Investigation (RSI) experiment is funded by DLR Bonn under grants 50QM1002 (TPA, BH) and 50QM1004 (MP, MH, ST, MKB) and under a contract with NASA (SWA, JDA). We thank T. Morley (ESOC) for valuable comments and all persons involved in Rosetta at ESTEC, ESOC, ESAC, JPL and the ESTRACK and DSN ground stations for their continuous support.

References

Aster, R. C.; Borchers, B. & Thurber, C., Parameter Estimation and Inverse Problems, *Elsevier Academic Press,* 2005

Baer, J., S. Chesley and D. Britt, Eds., Asteroid masses V1.0 EAR-A-COMPIL-5-ASTMASS-V1.0, Nasa Planetary Data System, 2009.

Baer, J., S.R. Chesley, R.D. Matson, Astrometric masses of 26 asteroids and observations on asteroid porosity, Astron. J. 141:143, (12pp), 2011.

Boehm, J., Werl, B., and Schuh, H., 2006a, “Troposphere mapping functions for GPS and very long baseline interferometry from European Centre for Medium-Range Weather Forecasts operational analysis data,” J. Geophys. Res.,

Buttkus, B., Spectral analysis and filter theory in applied geophysics, *Springer Verlag, Berlin, Heidelberg,* 2000

Carry, B. et al. (24 Co-authors), Physical properties oft he ESA Rosetta target asteroid (21) Lutetia, Astron. Astrophys. 523, A94, 2010.

Chao, C. C., A Model for Tropospheric Calibration from Daily Surface and Radiosonde Balloon Measurements,*Technical Memorandum 391-350, Jet Propulsion Laboratory, Pasadena, California, USA,* 1972

Fienga, A., H. Manche, J. Laskar, and M. Gastineau, INPOP06: a new numerical planetary ephemeris, Astronomy and Astrophysics, Volume 477, pp.315-327, 2008.

Fienga, A., H. Manche, P. Kuchynka, J. Laskar, M. Gastineau, Planetary and Lunar ephemerides, INPOP10A, arXiv.org > astro-ph > arXiv:1011.4419, 2010.

Folkner, W. M.; Williams, J. G. & Boggs, D. H., The planetary and Lunar Ephemeris DE 421, *JPL IOM, 343R-08-003, 2008.*

Folkner, W.M., J.G. Williams and D.H. Boggs, The Planetary and Lunar Ephemeris DE421, IPN Progress Report 42-178, August 15, 2009.

Häusler, B., W. Eidel, R. Mattei, S. Remus, M. Pätzold & s. Tellmann, The Planetary Atmospheric Doppler Effect in a Relativistic Treatment, *FORSCHUNGSBERICHT, , LRT 9-FB-5*, 36, 2007.

Ifadis, I., The Atmospheric Delay of Radio Waves: Modeling the Elevation Dependence on a Global Scale, *Technical Report no. 38L, School of Electrical and Computer Engineering, Chalmers University of Technology, Göteborg, Sweden,* 1986.

Lamy P., G. Faury, L. Jorda, M. Kaasalainen, and S. F. Hviid., Multi-color, rotationally resolved photometry of asteroid 21 Lutetia from OSIRIS/Rosetta observations, 2010.

McCarthy, D. D. & Petit, G., IERS Conventions (2003), *International Earth Rotation and Reference System Service (IERS), IERS Technical Note; N0. 32* , 203.

Pätzold, M. et al., MaRS : Mars Express Radio Science Experiment, ESA-SP 1291, 217-248, 2009. Häusler, B. et al., Radio science investigations by VeRa onboard the Venus Express spacecraft, Planetary and Space Science 54, 1315–1335, 2006.

Pätzold, M., T. P. Andert, B. Häusler, S. Tellmann, J. D. Anderson, S. W. Asmar, J.-P. Barriot, and M. K. Bird, Pre-flyby estimates of the precision of the mass determination of asteroid (21) Lutetia from Rosetta radio tracking, Astronomy and Astrophysics, Volume 518, id.L156, 2010.

Petit, G. & Luzum, B. IERS Conventions (2010) International Earth Rotation and Reference Systems Service (IERS), 2010

Press, W. H.; Teukolsky, S. A.; Vetterling, W. T. & Flannery, B. P., Numerical Recipes in Fortran, *Cambridge Univ. Press, Cambridge,* 1986

Saastamoinen, J. et al., Atmospheric Correction for the Troposphere and Stratosphere in Radio Ranging Satellites, *The Use of Artificial Satellites for Geodesy, American Geophysical Union, Washington D. C.,* 1972, 247-252

Schüler, T., On Ground Based GPS Tropospheric Delay Estimation, *PhD-Thesis, Universität der Bundeswehr, München,* 2001

Sierks et al., Science this volume, 2011.

Weiss, B.P., L.T. Elkins-Tanton, M.A. Barucci, H. Sierks, M. Pätzold, C. Snodgrass, S. Marchi, I. Richter, P.R. Weissman, M. Fulchignoni and R.P. Binzel, Evidence for thermal metamorphism or partial differentiation of asteroid 21 Lutetia from Rosetta, 42nd Lunar and Planetary Science Conference, 2077, (2011)..